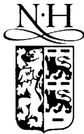
ELSEVIER

Nuclear Instruments and Methods in Physics Research B 175–177 (2001) 274–279

NIM B
Beam Interactions
with Materials & Atoms

www.elsevier.nl/locate/nimb

Ar-implanted epitaxially grown HgCdTe: evaluation of structural damage by RBS and TEM

M.H. Aguirre [a,*], H.R. Cánepa [b]

[a] CONICET and Laboratorio de Química de Estado Sólido, Departamento de Química Inorgánica, Facultad de Cs. Químicas, Universidad Complutense, Av. Complutense s/n, 28040 Madrid, Spain

[b] Programa de Investigación en Sólidos – PRINSO-CONICET-CITEFA, Zufriategui 4380, 1603 Villa Martelli, Buenos Aires, Argentina

Abstract

Mercury cadmium telluride alloys $Hg_{1-x}Cd_xTe$ (MCT) is an important semiconductor material used in infrared photovoltaic detectors. Although ion implantation is a widely used technique in the manufacture of devices based on MCT, a detailed understanding of the n-type behaviour of the unannealed damage region has not yet been established. In the present paper n on p junctions were formed by Ar^{++} implantation on MCT(1 1 0) grown by isothermal vapour phase epitaxy method (ISOVPE). Comparison of the structural damage after implantation is evaluated by Rutherford backscattering spectrometry (RBS) and transmission electron microscopy (TEM) measurements for different doses. Damage distribution presents two peaks and defects are primarily vacancy dislocation loops in the first region. The observed n-type behaviour after implantation is attributed to the generation and diffusion of Hg from the damage region. © 2001 Elsevier Science B.V. All rights reserved.

PACS: 61.80; 61.72.Uv; 61.82.Fk; 61.72.Ff
Keywords: HgCdTe; Ion implantation; RBS; TEM; Defects; Dislocations

1. Introduction

Mercury cadmium telluride alloys $Hg_{1-x}Cd_xTe$ (MCT) are semiconductors with a band gap which can be varied from approximately −0.3 to 1.6 eV as the variable composition x goes correspondingly from 0 to 1 [1]. This has opened up the possibility of designing infrared detectors in MCT tuned for the 3–5 μm or the 8–14 μm wavelength atmospheric window.

Studies of junction formation mechanisms in implanted MCT have led to different hypothetical models consistent with experimental observations [2–5]. Junction formation and stability is a key issue related to the improvement of infrared MCT photodiode technology. In Te-rich MCT the Hg vacancy can be quite high. As these vacancies are doubly negative charged [6] it determines the p-type conductivity of undoped MCT. Junction formation occurs when excess Hg interstitials recombine with Hg vacancies. This excess Hg

* Corresponding author. Tel.: +34-91-394-4214; fax: +34-91-394-4352.
E-mail address: aguirrem@eucmos.sim.ucm.es (M.H. Aguirre).

0168-583X/01/$ - see front matter © 2001 Elsevier Science B.V. All rights reserved.
PII: S 0 1 6 8 - 5 8 3 X (0 0) 0 0 6 3 2 - 7

interstitial can be injected by different processes including ion implantation [4].

This report describes the n-on-p junction formation by Ar^{++} implantation with different energies and doses, in order to determine the predominant defects and their distribution.

2. Experimental

Undoped p-type MCT was grown at PRINSO by the ISOVPE method [7] onto (1 1 0) CdTe substrates provided by eV PRODUCTS Division. Substrates were chemically polished with a solution of 2% bromine–methanol prior to growth.

Implantation of Ar^{++} was performed at room temperature with energies between 300 and 360 keV, doses between 10^{13} and 10^{16} Ar^{++}/cm^2 and ion current densities lower than 1.0 $\mu A/cm^2$. RBS was used to evaluate the crystallinity of samples (virgin and implanted) and to obtain the density of defect distribution. Table 1 summarises the stoichiometry of samples and implantation data. All samples show p-type conduction (10^{15} cm^{-3} $< p < 10^{17}$ cm^{-3}) before implantation and n-type conduction ($>10^{16}$ cm^{-3}) after implantation.

RBS measurements were performed by ^4He beam at different energies in a 3 MeV Tandetron accelerator system at UFRGS – Porto Alegre, Brazil.

Samples for TEM were thinned by a precision ion polishing system (PIPS), Model Gatan 691, at very low voltage ($V^+_{Ar} < 4$ kV) in planar view. The TEM examination was performed in a JEOL 2000 FX microscope equipped with a LaB_6 emitter and operating at 200 kV. An EDX spectrometer (Link Pentafet Model 5947, Oxford Microanalysis Group) was used to check the composition in TEM examinations. The maximum thickness through which defects could be imaged under this condition was $\approx$1500 Å from the surface.

3. Results

Figs. 1(a) and (b) show the RBS spectra in random and channeling conditions along the [1 1 0] axis for samples: VPE 202 examined at 1.2 MeV and VPE 62 examined at 760 keV ^4He, in virgin and implanted parts.

No amorphisation is observed and the surface region remains a nearly perfect crystal (Hg and Te peaks are clearly detected). The channeling spectra of the implanted samples show a high dechanneling rate at increasing implanted fluences. This means that the disorder is high at high implantation doses. The χ_{min} was 10% for samples as-grown and between 20% and 30% for implanted samples.

To evaluate the density of defects as a function of depth $N_D(z)$, we calculate this density from the expression

$$N_D(z) = \frac{-1}{\sigma}\frac{d}{dz}\left\{\ln\left[\frac{\chi_R(z)-\chi_V(z)}{1-\chi_V(z)}\right]\right\}^{-1}. \quad (1)$$

We assumed that χ_R and χ_V can be directly extracted from RBS and channeling data [8] at

Table 1
Description of samples: implantation conditions and sample stoichiometry

Samples (1 1 0)	Implantation conditions		Composition 'x' (before implantation)
	Dose (Ar^{++}/cm^2)	Energy (keV)	
VPE 76	0	0	0.17
VPE 202	10^{13}	360	0.13
VPE 78 A	10^{13}	360	0.29
VPE 87	10^{14}	300	$0.16 < x < 0.24$
VPE 62	10^{15}	300	0.22
VPE 78 B	10^{15}	360	0.29
VPE 77	10^{16}	360	0.29

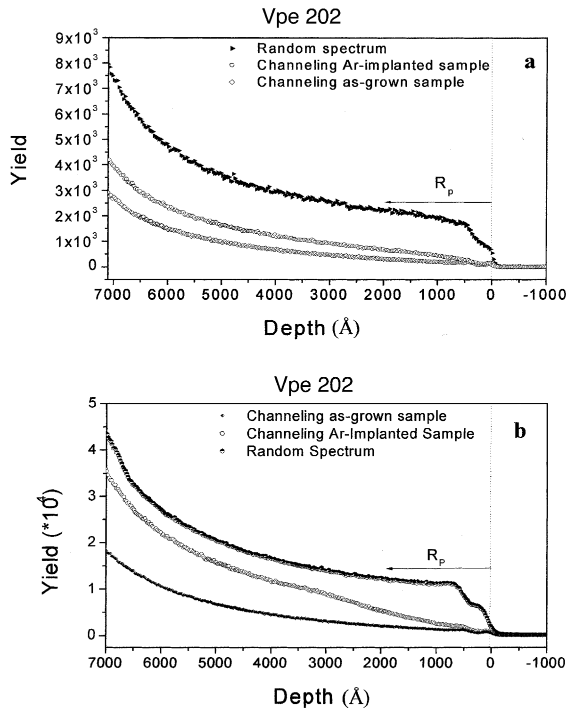

Fig. 1. RBS spectra in random and channeling conditions for (a) VPE 202 and (b) VPE 62. Implanted samples under conditions described in Table 1.

implanted (χ_2) and virgin sample (χ_1) as a function of depth as is customary [9]. The logarithms of the relative minimum yield 'r',

$$r = \frac{\chi_2 - \chi_1}{1 - \chi_1}, \tag{2}$$

was fitted with a sixth- to eighth-order polynomial as a function of depth. Eq. (1) was analytically solved and the damage depth profile was obtained. These results are shown in Figs. 2(a) and (b). The projected range (R_p) was obtained from the TRIM-code [10] for each implantation condition.

TEM analysis of implanted samples exhibits dislocation loops in all cases, while in as-grown samples we observed high crystallinity or a few and small number of dislocation lines (as shown in Fig. 3(a)). The planes of some dislocation loops have been determined using the stereographic view and they were all found to lie in {1 1 0} or {1 1 1} family planes. The nature of these loops (interstitial or vacancy-type) was identified by the classical internal–external contrast technique [11,12], taking pictures at $\pm\boldsymbol{g}$ diffraction vector (with $\boldsymbol{s} > 0$). This study has allowed to identify the loops as predominantly vacancy type.

In Figs. 3(b)–(e) we observe loops with increased radius at increased doses in all implanted samples. This characteristic is particularly remarkable if we compare the micrographs of implanted samples with doses 10^{13} and 10^{14} Ar^{++}/cm^2. For doses of 10^{13} the loop radii are between 136 Å $< R <$ 455 Å (small size) and for 10^{14}, 400 Å $< R <$ 3000 Å (medium size). For samples implanted with doses 10^{15} and

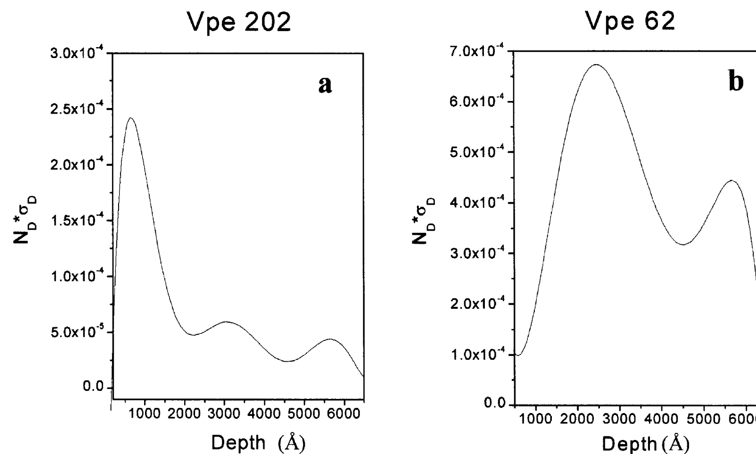

Fig. 2. Defects profile extracted from calculus of Eq. (1) for samples: (a) VPE 202 and (b) VPE 62.

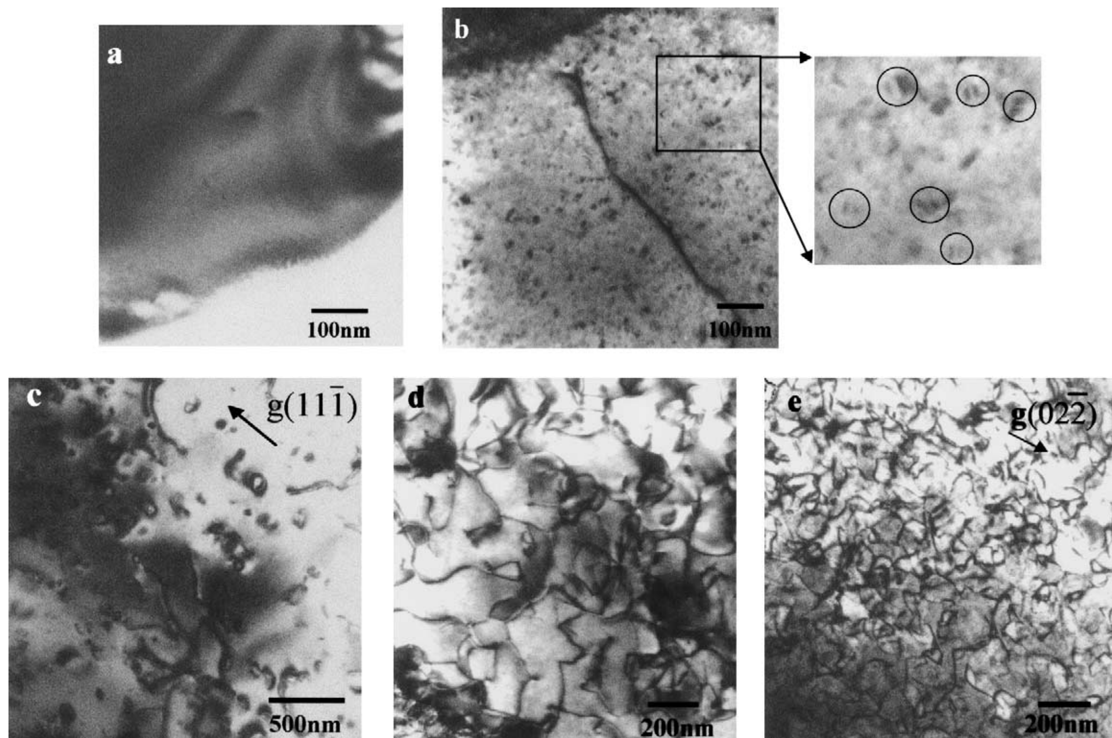

Fig. 3. TEM micrograph of as-grown and implanted samples (from 10^{13} to 10^{16} Ar^{++}/cm^2): (a) VPE 76 as-grown, (b) VPE 78 A, (c) VPE 87, (d) VPE 78 B and (e) VPE 77 (see Table 1).

10^{16} Ar^{++}/cm^2 dislocation loops are mixed and overlapped, their interaction gives different contrasts and makes definition of a visible radius and a round shape impossible.

We have also evaluated the change in mercury composition in implanted samples (before and after implantation) and in as-grown samples (before and after thinning). There is no change of Hg composition in the thinning process of the as-grown samples. However, we could observe that the Hg percent decreases after implantation and also decreases as the dose increases.

4. Discussion

From calculus extracted at the RBS spectra (Fig. 2), we can predict that there are two regions of defects, one of them between 1000 and 2000 Å and another between 4000 and 6000 Å approximately. The first peak of defects corresponds to dislocation loops as we have proved by TEM. This is possible because we can analyse this region in planar view samples by this technique.

On the other hand, we identified dislocation loops as predominantly vacancy type (with the method described in Section 2). This is corroborated by the in situ microanalysis that shows a decreasing Hg percentage with increased implantation doses (in the region of 0–2000 Å depth). Besides, these data are in accordance with mono-energetic positron beam measurements by Uedono et al. [13].

One part of excess initial defects takes place in the process of ion-induced surface evaporation. Nevertheless Hg interstitial generation during implantation must be stronger than Hg losses in surface evaporation. Besides, Ebe et al. [5] have found a narrow p-type region between 1000 and 2000 Å in the n^+ region in samples implanted with Ar^+. This p-type region coinciding with the first peak of defects (Fig. 2) and TEM imaging and

EDX measurements of this report is due to the generation of many Hg vacancies during implantation and the inability of implants to substitute Hg in the sublattice.

For MCT, since the binding energies of atoms are low as compared with those for single-element semiconductors, extended defects such as dislocation loops and stacking faults are easily introduced at room temperature [14]. In addition, because of ionic forces between atoms, the recombination of defects is more likely to occur. This is the possible reason why this material is not amorphised under implantation.

Using TEM, Bubulac et al. [15] and Schaake [2] reported that dislocation loops appeared for B^+ implanted in MCT with a dose $>10^{15}$ cm^{-2}. Schaake [2] showed that dislocation loops are predominantly interstitial type and they are most likely to be introduced by the agglomeration or the clustering of mobile defect such as I_{Hg}. But, this is in contradiction with the present experiment, and by Uedono et al. [13] and by Ebe et al. [5], where the major species of vacancy-type defects in the first region (0–2000 Å) are likely to be open spaces associated with extended defects. This is suggested by the trapping of positrons by vacancy-type defects [13] and for the slightly p-type region near 1000 Å from the surface [5].

Another argument which supports the idea that the loops are vacancy type in the first region is the Cascade Theory in the context of the irradiation process [16–18].

To conclude this section, we wish to comment that the second peak of the defects profile in Fig. 2 could be attributed to a second region of defects, possibly dislocation loops of the interstitial type. Lévêque et al. [19] have carried out diffuse X-ray scattering measurements in samples implanted with Al^{2+} (320 keV) and they have detected dislocation loops from 2000 to 5000 Å depth. To confirm this fact, cross-section thinned samples are going to be prepared for examination by TEM.

5. Conclusions

- This paper reports on the structural damage of Ar-implanted epitaxially grown MCT. From TEM observations our data indicate that the predominant defects which are formed at 300–360 keV implants are dislocation loops. They have been identified as vacancy type in the subsurface region (0–2000 Å). Measurements of loop radii for different implantation doses showed that loop radius increases as the implantation dose increases.
- Evaluations of the loss of Hg from the semiconductor surface have proved that there is no change of Hg composition in the thinning process, but Hg percentage decreases as the implantation dose increases.
- The observed n-type behaviour after the implantation damage is not due to dislocation but is attributed to the generation and diffusion of Hg from the damaged region towards the inside of the crystal during implantation. This could be the reason why junctions extend much deeper into the crystal ($\geqslant 1$ μm for unannealing samples and $\geqslant 2$ μm for annealing samples) [15] than in the doped layer.

Acknowledgements

The authors would like to thank Ing. Javier Fernandez and Dr. Alberto Filevich for sample implantation at Tandar Lab. (CNEA) Argentina, and Dr. Moni Behar for allowing us to perform the RBS measurements at UFRGS (Brazil). The authors are also indebted to Professor Miguel Ángel Alario-Franco for providing facilities at Microscopy Centre "Luis Brú" at UCM (Spain).

References

[1] J. Brice, P. Capper, Properties of Mercury Cadmium Telluride, INSPEC, The Institution of Electrical Engineers, 1987.
[2] H. Schaake, J. Vac. Sci. Technol. A 4 (4) (1986) 2174.
[3] L.O. Bubulac, J. Crystal Growth 86 (1988) 723.
[4] B.L. Williams, H.G. Robinson, C.R. Helms, J. Electron. Mater. 27 (6) (1998) 583.
[5] H. Ebe, M. Tanaka, Y. Miyamoto, J. Electron. Mater. 28 (6) (1999) 854.
[6] H.G. Robinson, D.H. Mao, B.L. Williams, S. Holander-Gleixner, J.E. Yu, C.R. Helms, J. Electron. Mater. 25 (8) (1996) 1336.

[7] J.G. Fleming, D.A. Stevenson, J. Crystal Growth 82 (1987) 621.
[8] C. Bahir, R. Kalish, J. Appl. Phys. 54 (6) (1983) 3129.
[9] M.L. Swanson, Rep. Prog. Phys. 45 (1982) 47.
[10] C.J.F. Ziegler, J.P. Biersack, TRIM-95 Program (transport of ion in matter).
[11] P. Hirsch, A. Howie, R. Nicholson, D. Pashley, M. Whelan, in: Electron Microscopy of Thin Crystal, Butterworth, London, 1969.
[12] J.W. Edington, Interpretation of Transmission Electron Micrograph, Philips Technical Library, Monographs in Practical Electron Microscopy in Material Science, Part 3, 1975.
[13] A. Uedono, H. Ebe, M. Tanaka, R. Suzuki, T. Ohdaira, S. Tanigawa, T. Mikado, K. Yamamoto, Y. Miyamoto, Jpn. J. Appl. Phys. 37 (1998) 3910.
[14] G.L. Destefanis, J. Crystal Growth 86 (1988) 700.
[15] L. Bubulac, W. Tennant, R. Riedel, T. Magee, J. Vac. Sci. Technol. 21 (1) (1982).
[16] M. Jenkins, J. Nucl. Mater. 216 (1994) 124.
[17] R.S. Averback, J. Nucl. Mater. 216 (1994) 49.
[18] W. Jäger, K.L. Merkle, Philos. Mag. A 44 (1981) 741.
[19] P. Lévêque, A. Declémy, P.O. Renault, Nucl. Instr. and Meth. B 168 (2000) 40.